Journal of Fluid Science and Technology

Vol.2, No.1, 2007

Efficient Immersed Boundary Method for Strong Interaction Problem of Arbitrary Shape Object with the Self-Induced Flow*

Yoshihiko YUKI**, Shintaro TAKEUCHI** and Takeo KAJISHIMA**

** Department of Mechanical Engineering, Osaka University

2-1 Yamada-oka, Suita-city, Osaka 565-0871 JAPAN

Abstract

An immersed boundary method is improved and applied to 2-D flow fields involving a single stationary/moving object. The present immersed boundary method employs a body force proportional to a solid volume fraction for coupling the solid and fluid motions at the interface. A hyperbolic-tangent function is newly introduced as a surface digitiser for computing the volume fractions at the interface cells, and this improvement is proved to be efficient for problems involving arbitrary shape object. The present method is applied to a uniform flow field around a circular cylinder and an interaction problem of fluid and free-falling object. The computational results are found to agree with the results by the different methods of the present authors and the results reported in the literatures. Also the computation time is considerably cut down compared to the other methods by the series of improvements to the immersed boundary method.

Key words : Immersed Boundary Method, Fluid-Solid Interaction, Non-Spherical Object, Surface Digitiser, Computational Fluid Dynamics

1. Introduction

Solving interaction problem of different continua is one of the most challenging subjects in numerical simulation as the system usually involves different time scales corresponding to the different phases within it. Many important and critical subjects are known in the engineering field, particularly concerning fluid-solid interaction problem. The examples include oscillation of fuel rods in a nuclear reactor, clustered behaviours of particles in the atmosphere/chemical chamber and falling leaves showing swinging and rotating motions.

The particular difficulty in the fluid-solid analyses lies in the implementation of the momentum exchange in the computational procedure at the moving interface. Body-fitted coordinate in curvilinear coordinate system may be the most widely-employed choice for the numerical simulation of the flow around the object. The main advantage of this method is that the flow (Eulerian variables) can be resolved along the object surface (Lagrangian variables) and therefore high resolution near the boundary layer is expected. However, due to the requirements by the mesh generation, application of the method is not straightforward when objects with complex geometry are included. Also, re-generation of computational grid is needed every time the objects translate, which often increases the computation load significantly. This problem is partially resolved by employing a body-fixed non-inertial treatment[1),(2)] or arbitrary Lagrangian-Eulerian approach[3)]. However, these approaches resolving the flow field with body-fitted coordinates are no longer applicable to the system where free movements of poly-sized particles (meshing over multiple-connected regions) or contacting of the multiple objects is dominant.

On the other hand, use of rectangular grid for analysis of flow field around arbitrary shape object has been drawing attention due to the simple numerical treatment and low computation cost. Generally, in this approach, the object of arbitrary shape is resolved by rectangular grid, and the effect of the interface of the two phases is incorporated into the dynamics of both

*Received 12 June, 2006 (No. 06-0044)
[DOI: 10.1299/jfst.2.1]

phases through a specially designed interaction force at the computational cells clipped by the "immersed boundary".

Form of the interaction force allows some arbitrariness. Peskin[4] has proposed a feedback force for his immersed boundary method (IBM). The main idea of his method is to use a rectilinear Eulerian grid for the fluid phase together with a Lagrangian representation for the immersed boundary (zero-thickness interface) at the object surface. The fluid and solid phases share the physical properties at the immersed boundary by mutual interpolation between the Eulerian and Lagrangian references via a pseudo delta function as a weight function. The method has demonstrated its versatileness through application to a number of problems including blood flow in a heart[4] and deformable biological cells experiencing shear[5]. However, this method has two adjustable parameters for the spring-dashpot feedback force, which are unable to be determined uniquely. Also, it is perhaps due to a problem in the interpolation procedures at the thick-less immersed boundary that flux leaks from the higher pressure side to the lower pressure side across the boundary[6].

IBM with direct-forcing method proposed by Mohd-Yusof[7] is more straightforward than the feedback forcing method. In this method the object surface passing through the computational cells is enforced with Dirichlet conditions for velocities at the object surface. The surface velocities are determined by interpolations between velocities defined at the object surface (Lagrangian point) and the neighbouring grid points (Eulerian point). This interpolation procedure is repeated for all the velocity components and also from Eulerian reference back to the Lagrangian reference. Therefore, for accurate prediction of fluid-object interaction, the crossing patterns of the interface over the cell need to be classified throughly. However the accuracy of the interpolation changes from a multi-linear form to a simply linear form interchangeably depending on the number of donor grid points available for the interpolation. It is perhaps due to this delicate nature of the interpolation that a less number of applications[7],[8] are found for flow analyses involving moving boundaries than the feedback approach.

The present authors have independently developed an immersed boundary method of body force type[9]. In this method, the force between the solid and fluid is modelled by a volume function of the solid volumetric fraction and the relative velocities of the two phases. The model ensures no momentum leakage between the phases, as the rectilinear Eulerian grid is shared with the object for representing both fluid and object's behaviours and, therefore, no interpolation is performed between the phases. This idea enabled high speed computation compared to the above two forcing methods, and this method has been applied to direct numerical simulation (DNS) of particle-induced turbulence of a total number of $O(10^3)$ spherical particles[10]. However, it should be noted that the formulation of this body-force method has been specifically designed for circular or spherical objects.

The present study aims to show a series of improvements for our body-force IBM to allow non-spherical geometry (of any dimensions) for object and to generalise the numerical implementation for identifying the immersed boundary (surface digitiser). Also, for further reduction in computation cost, high compatibility with the fast Fourier transform (FFT) is demonstrated. The present method is applied to 2-D flow fields to assess the validity and applicability of the method. A direct-forcing IBM and a non-inertial approach are tested for comparison with the present body-force IBM in a uniform flow field around a circular cylinder and for a free-falling object experiencing alternating acceleration and deceleration in a fluid.

2. Immersed boundary method of body force type

2.1. Basic equations

The governing equations for fluid flow are the equation of continuity and the Navier-Stokes (N-S) equations:

$$\nabla \cdot \boldsymbol{u}_f = 0\,, \tag{1}$$

$$\frac{\partial \boldsymbol{u}_f}{\partial t} + \boldsymbol{u}_f \cdot \nabla \boldsymbol{u}_f = -\frac{1}{\rho_f}\nabla p + \nu_f \nabla \cdot \left[\nabla \boldsymbol{u}_f + (\nabla \boldsymbol{u}_f)^T\right], \tag{2}$$

where $\boldsymbol{u}_f$ denotes fluid velocity, p pressure. Density and kinematic viscosity of the fluid, ρ_f and ν_f, are constant throughout the present work. Cartesian grid is used for arrangement of the Eulerian variables.

Motion of object is simulated by solving the equations of linear momentum and angular momentum as follows:

$$\frac{d(m_p \boldsymbol{v}_t)}{dt} = \int_{S_p} \boldsymbol{\tau} \cdot \boldsymbol{n} dS + \boldsymbol{G}_p \,, \tag{3}$$

$$\frac{d(\boldsymbol{I}_p \cdot \boldsymbol{\omega}_p)}{dt} = \int_{S_p} \boldsymbol{r} \times (\boldsymbol{\tau} \cdot \boldsymbol{n}) dS + \boldsymbol{N}_p \,, \tag{4}$$

where $\boldsymbol{v}_t$ is translating velocity of the object, $\boldsymbol{\omega}_p$ angular velocity, m_p mass of the object, $\boldsymbol{I}_p$ inertia tensor, $\boldsymbol{G}_p$ external force, $\boldsymbol{N}_p$ external torque, S_p object surface, $\boldsymbol{n}$ unit vector in the normal outward direction at the surface, $\boldsymbol{r}$ relative position from the gravity centre to a point in the integral region.

2.2. Fluid-solid interaction model and numerical implementation

Momentum exchange at the fluid-solid interface, where a cell is partially occupied by a solid particle (intruder), is solved by immersed boundary method developed by Kajishima and coauthors[9),(10)]. This is briefly described in the following for the convenience of the subsequent sections.

A velocity field $\boldsymbol{u}$ is established through volume-averaging of local fluid velocity $\boldsymbol{u}_f$ and local particle velocity $\boldsymbol{u}_p$ in a cell, i.e.,

$$\boldsymbol{u} = (1 - \alpha)\boldsymbol{u}_f + \alpha \boldsymbol{u}_p \,, \tag{5}$$

where α ($0 \le \alpha \le 1$) is the local solid volume fraction in the cell. The particle velocity $\boldsymbol{u}_p$ can be decomposed into translating and rotating components as $\boldsymbol{u}_p = \boldsymbol{v}_t + \boldsymbol{r} \times \boldsymbol{\omega}_p$. The velocity field $\boldsymbol{u}$ is assumed to obey the following N-S equation:

$$\frac{\partial \boldsymbol{u}}{\partial t} = -\nabla P + \boldsymbol{H}_u + \boldsymbol{f}_p \,, \tag{6}$$

where $P = p/\rho_f$ and $\boldsymbol{H}_u$ contains convective and viscous terms as follows:

$$\boldsymbol{H}_u = -\boldsymbol{u} \cdot \nabla \boldsymbol{u} + \nu_f \nabla \cdot [\nabla \boldsymbol{u} + (\nabla \boldsymbol{u})^T] \,. \tag{7}$$

A time advancement scheme of $\boldsymbol{u}$ is expressed by the following equations:

$$\boldsymbol{u}^{n+1} = \boldsymbol{u}_I - \Delta t \nabla P + \Delta t \boldsymbol{f}_p \,, \tag{8}$$

$$\boldsymbol{u}_I = \boldsymbol{u}^n + \frac{\Delta t}{2}(3\boldsymbol{H}_u^n - \boldsymbol{H}_u^{n-1}) \,, \tag{9}$$

$$\boldsymbol{f}_p = \frac{\alpha(\boldsymbol{u}_p - \boldsymbol{u}_I)}{\Delta t} \,, \tag{10}$$

where superscripts represent time and Δt is time increment. The body force $\boldsymbol{f}_p$ accounts for the effect of the intruder on the fluid at the interface and inside the object. It should be noted that, at $\alpha = 0$ where zero interaction force ($\boldsymbol{f}_p$=0) is enforced, the above time-marching procedure turns into Adams-Bashforth method and the SMAC method for a single-phase fluid. The same force as Eq.(10) with the opposite sign applies to the fraction of the particle in the cell. The hydrodynamic tensions at the interface is replaced with the body force $\boldsymbol{f}_p$, and time advancement of the particle phase is completed by integrating the force over the volume of the particle as follows:

$$\frac{d(m_p \boldsymbol{v}_t)}{dt} = -\rho_f \int_{V_p} \boldsymbol{f}_p dV + \boldsymbol{G}_p \,, \tag{11}$$

$$\frac{d(\boldsymbol{I}_p \cdot \boldsymbol{\omega}_p)}{dt} = -\rho_f \int_{V_p} \boldsymbol{r} \times \boldsymbol{f}_p dV + \boldsymbol{N}_p \,. \tag{12}$$

The use of the same body force $\boldsymbol{f}_p$ for fluid and particle phases in a shared cell ensures no leakage in the momentum exchange between the phases.

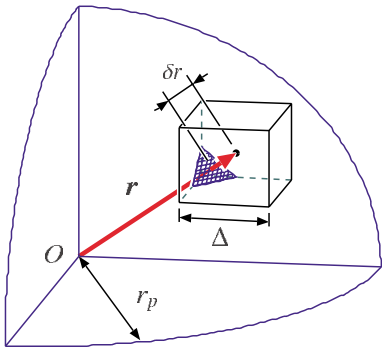

Fig. 1 A spherical object and a computational cell sharing a fraction of the interface.

The above scheme was validated through prediction of the drag force acting on a single spherical particle fixed in a space[9], together with vortex shedding in the wakes of individual particles for different Reynolds numbers[9),(10)].

In the present study, the numerical schemes are the same as Kajishima et al.[9], except that fast Fourier transform (FFT) is applied in the homogeneous directions of the computational domain, as explained in the following. Pressure P is determined apparently by the same procedure as SMAC with the intermediate velocity $\boldsymbol{u}_I$, where the scalar potential ϕ of SMAC is obtained by solving the following Poisson equation:

$$\frac{\partial^2\phi}{\partial x^2}+\frac{\partial^2\phi}{\partial y^2}=\frac{\nabla\cdot\boldsymbol{u}_I}{\Delta t}\,. \tag{13}$$

Solving this equation often consumes most of the computation time. However, by decomposing the above equation into the wave components with FFT in the homogeneous direction (y in the present example), the Poisson equation reduces in dimension into the following simultaneous linear equations:

$$\frac{1}{\Delta^2}\widehat{\phi}_{i-1,k_y}-\left(\gamma+\frac{2}{\Delta^2}\right)\widehat{\phi}_{i,k_y}+\frac{1}{\Delta^2}\widehat{\phi}_{i+1,k_y}=\frac{\nabla\cdot\widehat{\boldsymbol{u}_I}}{\Delta t}\,, \tag{14}$$

where $\gamma=-\dfrac{2(1-\cos k_y\Delta)}{\Delta^2}$,

enabling solution by considerably simplified algebraic operations for each wavenumber k_y independently. Here, $\widehat{\phi}$ and $\widehat{\boldsymbol{u}_I}$ are the Fourier coefficients of ϕ and $\boldsymbol{u}_I$, respectively, and Δ is cell size uniformly distributed over the computational domain. In the present study, the tri-diagonal matrix algorithm (TDMA) is employed. It should be noted that the compatibility with FFT is not always guaranteed in multi-phase flow simulations[7], as the scalar potential is often weighted according to geometric conditions with the intruder[11),(12)].

Throughout the present work, the variables are defined at collocated grid points, and a second-order accuracy is implemented for spatial and temporal discretisations.

2.3. Surface Digitiser

Interaction force $\boldsymbol{f}_p$ proportional to α works at the intruder surface and the fluid. In theory, α value could be determined uniquely from the geometric condition of the object surface at each interface cell. It has been proved that this process could be approximated efficiently by subdivision volume counting method[13] for the most fundamental case of spheres. However, the computational load in evaluating α increases with surface area in the whole domain, either by the increase in complexity of object's geometry or by the number of objects in the domain. Therefore development of an efficient algorithm for digitising interface is of great importance for efficient computation.

Figure 1 shows a schematic of a fraction of the interface between a sphere and a computational cell. Kajishima et al.[9] assumed that solid volume fraction distributes as a continuous

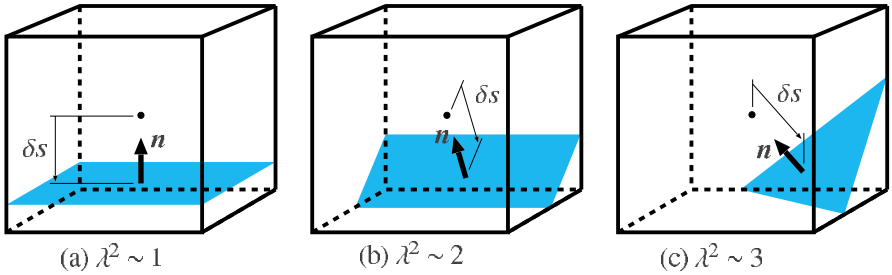

Fig. 2 Typical three patterns of interface in a cell classified by λ^2.

function over a cell, and approximated a digitised interface of a sphere (radius r_p) by a third order polynomial of $|\boldsymbol{r}| - r_p (\equiv \delta r)$, where $\boldsymbol{r}=(r_x, r_y, r_z)$ is a vector pointing to the centre of the cell from the particle centre. The functions for solid volume fraction were given as follows:

$$\alpha = \begin{cases} 1 & : \quad X < -1/2 \\ \dfrac{1 - \mathrm{sgn}(X) \cdot \left\{1 - (1 - 2|X|)^{\lambda^2}\right\}}{2} & : \quad -1/2 \le X < 1/2 \\ 0 & : \quad X \ge 1/2 \end{cases}, \tag{15}$$

$$X = \delta r / (\lambda \Delta) ,$$

$$\lambda = \frac{\max\left(|r_x + r_y + r_z|,\ |-r_x + r_y + r_z|,\ |r_x - r_y + r_z|,\ |r_x + r_y - r_z|\right)}{\sqrt{r_x^2 + r_y^2 + r_z^2}} , \tag{16}$$

where the function $\mathrm{sgn}(X)$ determines the sign of X. In addition to the above non-trivial formulae, α value needed to be evaluated at every definition point of the velocity components under staggered arrangement[9]. Also, the above method was specifically designed for a circular/spherical object.

In the present work, value of α is only evaluated at the collocation point for each cell. And the following hyperbolic-tangent function is proposed for evaluating volume fraction:

$$\alpha = \frac{1}{2}\left\{1 - \tanh\left(\frac{\delta s}{\sigma \lambda \Delta}\right)\right\} , \tag{17}$$

$$\lambda = |n_x| + |n_y| + |n_z| , \tag{18}$$

$$\sigma = 0.05(1 - \lambda^2) + 0.3 ,$$

where $\boldsymbol{n}=(n_x, n_y, n_z)$ is a normal outward unit vector at a surface element and δs is a signed distance from the cell centre to the surface element. A schematic is shown in Fig. 2. For a spherical object, Eq.(18) is proved to be equivalent to Eq.(16), however it should be noted that the new λ allows non-spherical object as well. And the authors' further investigation suggests that this digitiser has an essential advantage for flow analysis involving deformable objects. By the parameter λ, positions of the interface in a cell are classified into the following three typical cases:

1. $\lambda^2 \sim 1$: one full surface of the cell is included in the object (Fig.2(a))
2. $\lambda^2 \sim 2$: two neighbouring corners of the cell are included in the object (Fig.2(b))
3. $\lambda^2 \sim 3$: only one corner of the cell is included in the object (Fig.2(c))

The error in evaluating the particle volume in 3-D by the surface digitiser, Eq.(17), was found to be 0.26% and 0.43%, respectively, with 20 and 16 cells to cover the diameter of a spherical particle. We have compared the effect of Eq.(15) and (17) on a uniform flow field including a single circular cylinder, and confirmed that the change in algorithm for α caused negligible differences for the temporal fluctuations of drag and lift coefficients and transverse velocities 5 radii downstream of the cylinder. Also, due to the above simplified formulation, a high speed computation is expected for processing volume fraction. It was shown that the average elapsed time to process the present digitiser was reduced by 25% in comparison to that of the original digitiser Eq.(15). Also, by including the changes from the staggered grid system to

Table 1 Simulation conditions for uniform flow around a circular cylinder. Applied for both body-force and direct-forcing methods.

Number of Grids	$N_x \times N_y$	768×256
Spatial resolution	D/Δ	20
Reynolds number	$Re = DU_0/\nu_f$	50~300
Time increment	Δt	5×10^{-3}

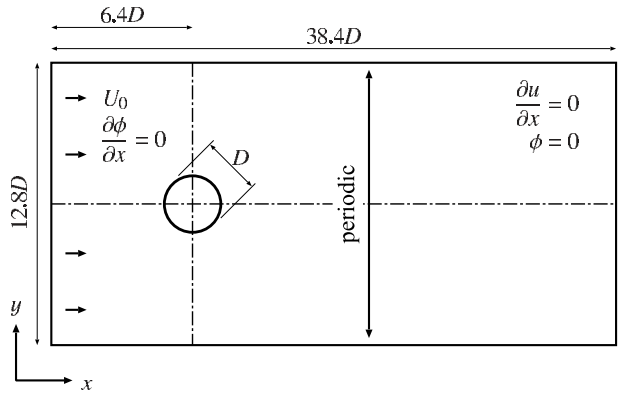

Fig. 3 Computational domain of the flow around a circular cylinder.

the collocated grid system, a total of 56% process time for the subroutine was cut down in a three-dimensional case.

3. Validation: Uniform flow around a circular cylinder

To assess the validity of the above formulae, the body-force method is compared with a direct-forcing method[12] in a flow field past a two dimensional circular cylinder.

In the present study, a direct-forcing method developed by the author[12] is applied. The forcing procedure of the direct-forcing method is mainly separated into two stages; first, the velocity of the fluid phase is updated by N-S equations, and second, the velocities at the grid points most neighbouring to the object surface are adjusted to those in the near field by interpolating the velocities at the second neighbouring grid point and at the object's surface (Lagrangian point). The direct-forcing method derives a pressure equation of spatially-weighted scalar potential, which rigorously satisfies the continuity equation consistent with the non-slip condition at the immersed boundary. This treatment substantially employs a wider stencil[12] than a conventional scheme with the same order of accuracy. However, it has essentially contributed to improving the direct-forcing approaches in flow resolution near the fluid-object interface[12]. Therefore, the accuracy of the body-force method is examined in the near field of the object with the simulation result of the direct-forcing method.

Figure 3 shows the computational domain and boundary conditions. For both methods, boundary conditions for the velocities are gradient free and periodic conditions at the out-flowing and lateral boundaries, respectively. At the inflow boundary a fluid is allowed to enter at a constant uniform velocity U_0 throughout the simulation. Pressure potential and its gradient are set to zero at the inlet and out-flowing boundaries. As the initial condition, u=U_0 and v=0 are given in the whole computational domain. All results presented in this section are obtained under the conditions set out in Table 1.

In Fig.4, vortical structures in the wake are compared at the same instance. The Reynolds number is 200. Colours represent intensity of vorticity, and the colour range is set to the same for the two cases. The similar flow structures are obtained for both cases. Also Strouhal numbers of the vortex shedding are found to be 0.198 and 0.202 for the present body-force method and the direct-forcing method, respectively.

Frequencies of vortex shedding are also studied for the Reynolds numbers ranging between 50 and 300, where a laminar vortex shedding is steadily observed[14]. Figure 5 is a

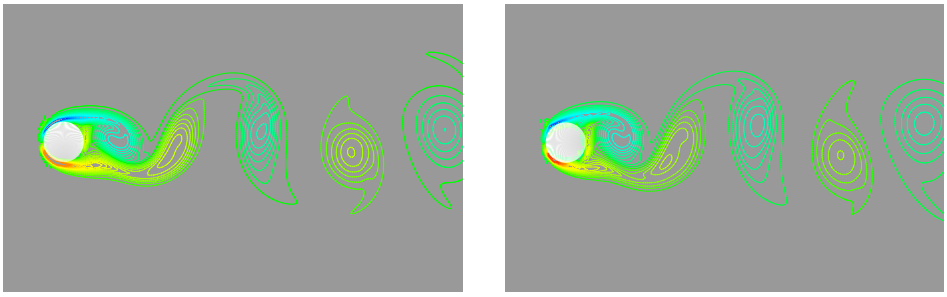

(a) (b)

Fig. 4 Instantaneous flow fields by (a)the present body-force method and (b)direct-forcing method. Both simulated at at *Re*=200.

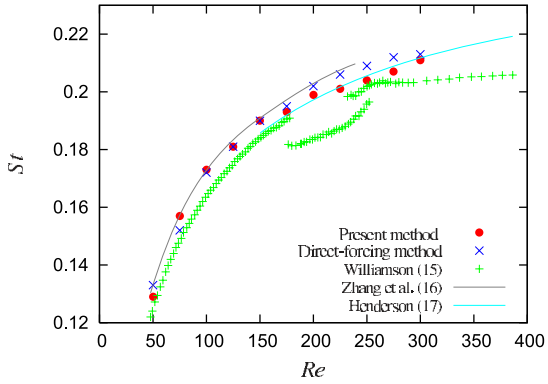

Fig. 5 Chart of Strouhal numbers of vortex shedding against Reynolds numbers.

chart of Strouhal numbers of observed vortices against the Reynolds numbers obtained by both body-force and direct-forcing methods. Also plotted in the same figure is the experimental[15] and simulation[16),(17)] results reported in the literatures. The discontinuities and hysteresis observed in the experimental results correspond to the onset of three dimensionality and transition to different 3-D vortical structures[15], suggesting that a comparison with the 3-D results in the higher *Re* range is less meaningful in this study. The present method shows particularly good agreement with the result by Zhang et al.[16] in the lower *Re* range and with that by Henderson[17] in the higher range.

The above results suggest that the present body-force method successfully reproduces the flow fields around a circular cylinder over the wide range of Reynolds number.

Table 2 compares computation times for 1000 time steps for body-force method and direct-forcing method[12]. Also, independent simulation without FFT was attempted and elapsed times are included in the same table. The computers used were Dell Precision 350 (scalar-type computer at Australian Partnership for Advanced Computing (APAC), 2.66 GHz Pentium4 × 152 nodes, over 800 Gflops in total) and NEC SX-5/128M8 (vector-type computer at Osaka University Cybermedia Center, 160 Gflops × 8 nodes in total). Both programs (body-force and direct-forcing method) were vectorised at rate of 99.9%. The present method offers reasonably fast computations for all the cases compared to the direct-forcing method irrespective of the use of FFT or the computers used. This is probably due to the reduction of computational load by FFT, a simple treatment of interface (the new digitiser) and a simple algorithm. Also, the present method with FFT exhibits particularly low cost on the vector-type computer in comparison to the other trials, which demonstrates the usefulness of vector-type computers for this type of problem. Even with the scalar computer, however, the present method is distinguished remarkably from the direct-forcing method. The results proves the advanced performance of the present method regardless of the use of FFT.

Table 2 Comparison of computation time for 1000 time steps for different methods on **[A]** NEC SX-5 (vector-type computer) and **[B]** Dell Precision 350 (scalar-type). A single processor was used on both computers.

[CPU sec /1000 steps]	**[A]**	(ratio to (b))	**[B]**	(ratio to (b))	**[B] / [A]**
(a) Present method with FFT	28	(1/32)	231	(1/6)	8.2
(b) Present method without FFT†	894	(1.0)	1366	(1.0)	1.5
(c) Direct-forcing method[12]	4258	(4.8)	16692	(12.2)	3.9

† Eq.(13) solved by SOR method

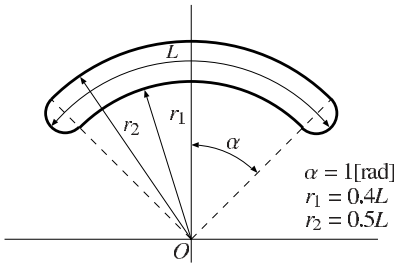

Fig. 6 Object shape and initial releasing orientation. Initially, gravity works in vertical downward in the figure.

4. Strong manoeuvre of free-falling object by self-induced vortices

To show the applicability of this method to moving boundary problems, behaviour of a non-spherical object suspended in a fluid is studied.

A U-shape object, shown in Fig.6, is released at zero velocity into a stationary fluid with its concave part facing vertical downward (as shown in Fig.6). These slender objects with a paired convex-concave part are expected to show unpredictable behaviours compared to simply-convex objects such as cylinder and symmetric airfoil.

The size of the computational domain is $20L$ in the vertical and $12.8L$ in the horizontal directions, and the numbers of cells in the respective directions are 800 and 512.

In the horizontal direction, a periodic boundary condition is used and FFT is applied. At the upper boundary, a modified traction-free condition[18] is applied, where the zero traction vector is solved together with the equation of continuity and p=0, assuming that the upper boundary is placed far enough from the object. The authors have found that this modified traction-free condition was particularly useful in simulating the in-coming flux from the external region across the boundary[18]. At the lower boundary, the gradient free condition is applied for pressure. Figure 7 shows a schematic of domain-switching which takes place when the gravity centre (G) of the object comes near to the lower boundary within a distance of $5L$; the upper part of the domain (length $9.5L$ from the upper boundary) is trimmed and appended to the bottom with a stationary fluid. In our preliminary study, it was confirmed that a flow field $5L$ below the object has been affected little by the object movements.

Spatial and temporal resolutions are L/Δ=40 and Δt=1 $\times$ 10^{-3}, respectively. Density distribution is uniform over the object volume, and density ratio ρ_s/ρ_f is varied in the range from 1.6 to 6. Reynolds number based on L and terminal velocity is set to 600. We have confirmed that the simulation results with the above spatial resolution agreed very well with those employing L/Δ=50.

For the two extreme density cases (ρ_s/ρ_f=1.6 and 6), some characteristic behaviours of free-falling U-shape object are observed, and the typical behaviours are visualised as sequential snapshots in Fig.8. The blue arrows in the figure point to the same direction with respect to the body centre to represent the instantaneous orientations of the object, and the green lines are trajectories of the object. Generally, the U-shape objects initially fall straight downward without changing the posture for some time (under asymptotic stable condition with the fluid force working on the object surface), and then, due to the development of vortices in the wake, it turns upside down involving a horizontal shift of the falling track (Fig.8(a)). After this tran-

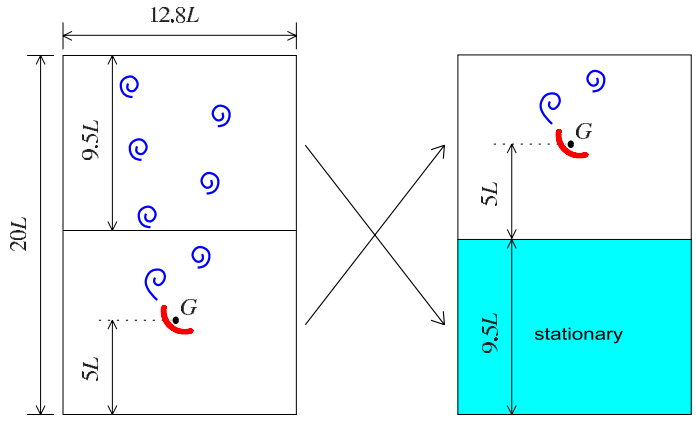

Fig. 7 Schematic of domain-switching.

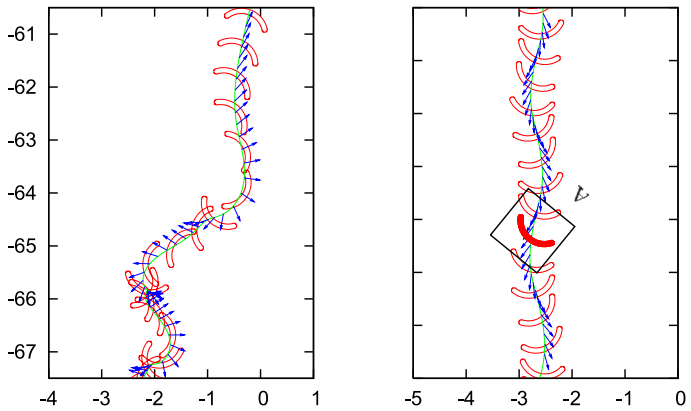

Fig. 8 Sequential snapshots of positions of the free-falling object of density ratio (a) 1.6 and (b) 6.

sition of motion, the objects fall swinging around its most stable position (with its concave part facing vertical upward) as shown in Fig.8(b). These behaviours, turn-over and swinging motion, were observed for all the density ratios investigated. The results have proved that the present method enables analysis of interaction problem showing a transition from a stable state to an unstable state involving vortex shedding from the object.

Behaviour of a single object in a fluid could be also described from a moving coordinate system fixed to the object. Therefore, simulation results with the present method is compared with those conducted independently in a body-fixed (non-inertial) frame of reference by the present authors[2]. The non-inertial treatment incorporates the effect of the frame transformation as apparent accelerations into the governing equations of fluid and object. The apparent accelerations are widely known as translational acceleration, centrifugal and Coriolis forces, and our non-inertial treatment includes the effect of angular acceleration as well. The main advantage of this approach is it does not restrict the spatial degree of freedom for the movement of the object; i.e. domain-switching is not necessary. Also, since boundary-fitted coordinate system is employed, the fluid grids are arranged along the object surface, and resolution of the flow field near the object is readily to be increased. The computational domain is a circle of $10L$ in diameter and a time increment of 2×10^{-4} is employed.

Figure 9 compares snapshots of velocity and pressure fields at the moments of the similar orientation and movement (Window A in Fig.8(b)) obtained by the present body-force IBM and the non-inertial approach[2]. The objects' angular velocities differed by no more than 3% for the two methods. The velocity field in Fig.9(b) was obtained by converting the non-inertial

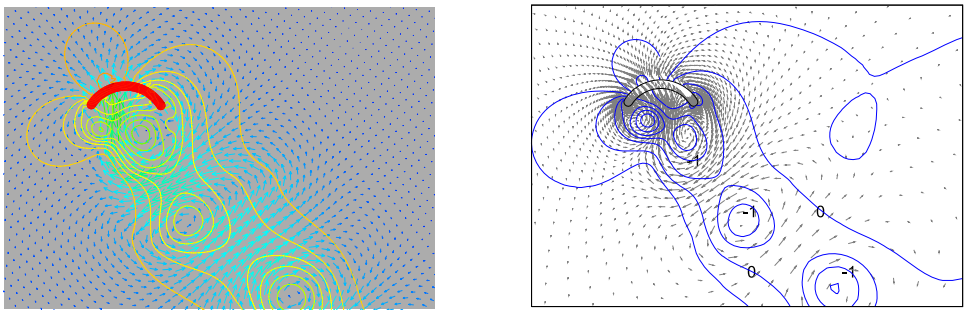

(a) (b)

Fig. 9 Comparison of instantaneous velocity and pressure fields obtained by two different methods; (a) the present immersed boundary method of body force type, (b) a body-fitted non-inertial treatment[2] and converted to the inertial frame.

velocity field into that of the inertial frame, and the flow field in Window A is also rotated to adjust the orientation to Fig.9(b). The velocity vectors in both Fig.9(a) and (b) are plotted every four and three points in both x-y and radial-circumferential directions, respectively. The figure suggests that the velocity and pressure fields predicted by the two methods are in good agreement over a spatial range covering the near and far fields of the object.

The present method has an advantage in time increment. The maximum angular velocity during the turn-over sequence (Fig. 8(a)) was found to be about 235 degrees per unit time, and the corresponding Courant number was well below 0.1 in the present simulation. The severeness of this angular velocity may be understood from the following estimate applied for the non-inertial system. With the same time increment (1×10^{-3}), the object in the non-inertial space would experience a Courant number 0.82 based on Δ and the rotation speed at the point $5L$ away from the gravity centre. The result suggests that the present body-force IBM also exhibits strong numerical stability with a relatively large time increment.

5. Conclusions

Applicability of our immersed boundary method of body force type was explored with a number of improvements in the interface treatment and computation efficiency.

The authors proposed simplified formulae for surface digitiser in conjunction with a new hyperbolic-tangent function for calculating solid volume fraction at the interface cells. This improvement enabled application of the present immersed boundary method to objects of non-spherical geometry with high efficiency. This treatment applies to any crossing patterns of the interface in a cell, and therefore, uniquely determines the interaction force at the immersed boundary without problem-dependent parameters or arbitrariness in interpolation procedure. Also the authors showed the strong compatibility of our immersed boundary method with the fast Fourier transform and demonstrated a significant improvement in computation speed.

The validity of the present surface digitiser was established through comparison with the simulation results by different numerical method in a uniform flow field around a fixed circular cylinder. The frequencies of vortex shedding agreed with the results reported in the literatures over a wide range of Reynolds number. The body-force immersed boundary method was also applied to an interaction problem between fluid and free-falling object which exhibits a transition from a stable state to an unstable state involving vortex shedding from the object. The validity of the moving boundary problem was demonstrated through comparison with an independent simulation result in a boundary-fitted non-inertial frame of reference. Also, the present immersed boundary method was found to be considerably efficient in computation with much higher computation speed with less possibilities of numerical instability.

Therefore, the present body-force immersed boundary method was successfully proved to be strong in solving flow field past a stationary/moving non-spherical object within a manageable computation time, and it promises to be a unique engineering tool practicable for

many challenging problems involving strong interactions between fluid and solid.

Acknowledgement

The authors gratefully acknowledge the Merit Allocation Scheme Grant of the Australian Partnership for Advanced Computing (APAC).

References

(1) Beddhu, M., Taylor, L. K. and Whitfield, D. L., "Strong conservation form of the incompressible Navier-Stokes equations in a rotating frame with a solution procedure ", *J. Comput. Phys.*, **128**, pp.427-437, 1996

(2) Takeuchi, S., Yamazaki, T. and Kajishima, T., "Study of Solid-Fluid Interaction in Body-Fixed Non-Inertial Frame of Reference", *J. Fluid Science and Technology*, **1-1**, pp.1-11, 2006

(3) Hirt, C. W., Amsden, A. A. and Cook, J. I., "An Arbitrary Lagrangian-Eulerian Computing Method for All Flow Speeds", *J. Comput. Phys.*, **14**, pp.227-253, 1974

(4) Peskin, C. S., "Flow patterns around heart valves: A numerical method", *J. Comput. Phys.*, **10-2**, pp.252-271, 1972

(5) Eggleton, C. D. and Popel, A. S., "Large deformation of red blood cell ghosts in a simple shear flow", *Phys. Fluids*, **10**, pp.1834-1845, 1998

(6) Yamada, Y., Takagi, S. and Matsumoto, Y., "Analysis of Immersed Boundary method applying to a lipid Bilayer" (in Japanese), *Proc. JSME 17th Comp. Mech. Conf.*, pp.191-192, Sendai, Japan, Nov, 2004

(7) Mohd-Yusof, J., "Combined immersed-boundary/B-spline methods for simulations flow in complex geometries", *CTR Annual Research Briefs*, NASA Ames/Stanford Univ., pp.317-327, 1997

(8) Kim, D. and Choi, H., "Immersed boundary method for flow around an arbitrary moving body", *J. Comput. Phys*, **212**, pp.662-680, 2006

(9) Kajishima, T., Takiguchi, S., Hamasaki, H. and Miyake, Y., "Turbulence structure of particle-laden flow in a vertical plane channel due to vortex shedding", *JSME Int. J. Ser. B*, **44**-4, pp.526-535, 2001

(10) Kajishima, T. and Takiguchi, S., "Interaction between particle clusters and fluid turbulence", *Int. J. Heat and Fluid Flow*, **23**(5), pp.639-646, 2002

(11) Takeuchi, S., Wang, S. and Rhodes, M., "Discrete element simulation of a flat-bottomed spouted bed in the 3-D cylindrical coordinate system", *Chemical Engineering Science*, **59**-17, pp.3495-3504, 2004

(12) Ikeno, T. and Kajishima, T., "Difference formula of Poisson equation consistent with an immersed boundary method" (in Japanese), *Trans. JSME Ser. B*, **70**-697, pp.2239-2245, 2004

(13) Tsuji, T., Narutomi, R., Yokomine, T., Ebara, S. and Shimizu, A., "Unsteady three-dimensional simulation of interactions between flow and two particles", *Int. J. Multiphase Flow*, **29**, pp.1431-1450, 2003

(14) Williamson, C. H. K., "Vortex Dynamics in the cylinder wake", *Annu. Rev. Fluid. Mech.*, **28**, pp.477-539, 1996

(15) Williamson, C. H. K., "The natural and forced formation of spot-like dislocations in the transition of a wake", *J. Fluid. Mech.*, **243**, pp.393-441, 1992

(16) Zhang, H., Fey, U., Noack, B. R., König, M. and Eckelmann, H., "On the transition of the cylinder wake", *Phys. Fluids*, **7**-4, pp.779-794, 1995

(17) Henderson, R. D., "Details of the drag curve near the onset of vortex shedding", *Phys. Fluids*, **7**-9, pp.2102-2104, 1995

(18) Takeuchi, S., Miyake, Y. and Kajishima, T., "On the numerical simulation of round jets of incompressible fluid", *Proc. of 3rd ASME/JSME Joint Fluids Eng. Conf. & FED Summer Meeting*, Paper No.6957, San Francisco, US, 1999